Paleoceanography and Paleoclimatology

RESEARCH ARTICLE
10.1029/2024PA005016

Modeling the Impact of Tides and Geothermal Heat Flux on the Climate of Early Earth

Benjamin Biewald[1,2], J. A. Mattias Green[3], Stefan Petri[1], and Georg Feulner[1,2]

[1]Earth System Analysis, Potsdam Institute for Climate Impact Research, Member of the Leibniz Association, Potsdam, Germany, [2]Institute of Physics and Astronomy, University of Potsdam, Potsdam, Germany, [3]School of Ocean Sciences, College of Science and Engineering, Bangor University, Bangor, UK

Key Points:

- First spatially resolved modeling of both tides and their impact on early Earth's climate
- Impact of tidal heating is strongest when altering ocean surface currents close to the sea-ice edge
- Tidal heating has only local impacts, but tidal mixing and geothermal heat flux influence global climate state

Correspondence to:

G. Feulner and J. A. M. Green,
feulner@pik-potsdam.de;
m.green@bangor.ac.uk

Citation:

Biewald, B., Green, J. A. M., Petri, S., & Feulner, G. (2024). Modeling the impact of tides and geothermal heat flux on the climate of early Earth. *Paleoceanography and Paleoclimatology*, *39*, e2024PA005016. https://doi.org/10.1029/2024PA005016

Received 10 SEP 2024
Accepted 20 NOV 2024

Abstract On early Earth increased rates of tidal energy dissipation are likely, but depend on the (unknown) distribution of continents. A stronger tidal heating could provide an additional energy source during times of substantially lower solar input. So far, the problem has been assessed in terms of the negligible contribution to Earth's global energy budget. Here we present a spatially resolved investigation of the impact of tidal heating, mixing, and geothermal heat on early Earth's climate. Using a random landmass distribution, tidal heating is calculated for three different rotation periods (12, 18, 24 hr) and fed into a climate model. For each rotation rate, three climate states with different atmospheric CO_2 levels are simulated. We find that, depending on the climate state, tidal heating can affect regional ocean dynamics and sea-ice cover. The impact is strongest when tidal heating alters sea-ice dynamics and meridional heat transport close to the sea-ice edge, but its global impact remains negligible with only small global mean changes in ice cover (0.3%) and temperature (<0.05°C). Adding tidal mixing and geothermal heat, however, leads to significant reduction in sea-ice cover of ∼11% and ∼19%, respectively, and thus to larger global warming. As we do not consider the dynamical effects of a higher rotation rate or different landmass distributions, this is only a first glimpse at the importance of tides for the climate of early Earth. Nevertheless, our results suggest that tides and geothermal heat are important for understanding regional climates and could have contributed to warming early Earth.

1. Introduction

Ocean tides influence a range of key Earth system processes (Green & Duarte, 2022). These include sustaining ocean primary production (Sharples et al., 2007; Tuerena et al., 2019), providing parts of the energy needed to maintain the climate-regulating overturning circulation in the ocean (Wilmes et al., 2021; Wunsch & Ferrari, 2004), and contributing to key evolution events (Balbus, 2014; Byrne et al., 2020). The drag introduced on Earth by the tides also forces Earth's spin to slow down, increasing day length, and causing the Moon to recede to conserve angular momentum of the system (Bills & Ray, 1999; Daher et al., 2021; MacDonald, 1964). Consequently, on early Earth the Moon was closer and the days much shorter. The Archean Eon spans nearly one third of Earth's history—from 4,031 to 2,500 Ma (million years ago)—and there is naturally uncertainty and a range of estimates of daylength for the Eon, from as short as 13 hr at 3,200 Ma (Eulenfeld & Heubeck, 2023) to 18 hr at the end of the Eon (Daher et al., 2021; Farhat et al., 2022). The tides are consequently the key controller of day length, which directly influence planetary habitability (Yang et al., 2014) as well as the timing of the oxygenation of the atmosphere (Klatt et al., 2021). An understanding of the evolution of tides and tidal drag through Earth's history is therefore key to understand other Earth system events.

The first order controller of tidal energetics is continental configuration, as for a fixed lunar distance, and hence tidal forcing, the tidal dissipation rates can vary up to three orders of magnitudes depending on continental configuration (Blackledge et al., 2020; Green et al., 2017). Consequently, even though the forcing was larger during the Archean, the tides may not have been more energetic. This is because the tides become resonant for specific basin geometries (Green, 2010), for example, the present day North Atlantic (Egbert et al., 2004; Green, 2010), and that effect can lead to larger amplification of the tide than the increase in forcing alone can do (Green et al., 2020).

The influence of the tides on the climate of early Earth has largely been assessed in terms of their contribution to the planetary energy balance (Barnes et al., 2008) in light of the Faint Young Sun Problem (FYSP) (Feulner, 2012). Even considering the larger tidal forcing on early Earth and the uncertainty with respect to continental configuration, however, the heating from tidal dissipation is expected to be negligible compared to the energy

input from the faint young Sun. Nevertheless, recent investigations of the geological imprint of ancient tides and the long-term evolution of the Earth-Moon distance have led to a renewed interest in the potential influence of tidal heating on the Hadean and Archean climate. For example, based on simple models for the long-term evolution of Earth's tides, Heller et al. (2021) argue that the global tidal dissipation, and hence heating, rate on early Earth may have been underestimated. They conclude that tides might have helped to keep surface water liquid for 220 Myr and could thus have been an important contribution to the planetary energy budget during the early Hadean. However, their approach necessarily neglects both tidally driven ocean dynamics and the influence of continental configuration on tidal dissipation (and is thus mainly a valid representation of deep aquaplanets), and the climatic consequences are assessed with a zero-dimensional gray atmosphere model ignoring internal climate dynamics and the ice-albedo feedback.

Here, we take the first step toward a more comprehensive assessment of the impact of tides on early Earth's climate by computing tidal energy dissipation rates from a spatially resolved tidal model for one particular continental configuration (broadly representative of an early Earth) and feeding the additional energy input as heat into a three-dimensional coupled climate model. This way, we can also investigate the effect of local tidal heating on ocean and sea-ice dynamics beyond the negligible impact on the global climate. Furthermore, we run additional sets of simulations including the effects of tides on vertical mixing in the ocean and with geothermal heat flux.

2. Methods

2.1. Tidal Modeling

The tide model simulations were done using OTIS, the Oregon State Tidal Inversion Software (e.g., Egbert et al., 2004; Green & Nycander, 2013). It has been used extensively for paleotidal simulations as far back as the Proterozoic (Green & Duarte, 2022; Green & Huber, 2013; Green et al., 2017, 2020). It solves the linearized shallow water equations:

$$\frac{\partial \mathbf{U}}{\partial t} + \mathbf{f} \times \mathbf{U} = -gH\nabla\left(\zeta - \zeta_{EQ} - \zeta_{SAL}\right) - \mathbf{F} \tag{1}$$

$$\frac{\partial \zeta}{\partial t} = -\nabla \cdot \mathbf{U} \tag{2}$$

Here, $\mathbf{U}$ is the depth integrated volume transport, H is water depth, $\mathbf{f}$ the Coriolis vector, g the gravitational constant, ζ the tidal elevation, ζ_{EQ} the equilibrium tidal elevation, and ζ_{SAL} the tidal elevation due to self-attraction and loading. The tidal drag is parameterized through two parts: $\mathbf{F} = \mathbf{F}_B + \mathbf{F}_{IT}$, where $\mathbf{F}_B$ is frictional losses due to bed friction and $\mathbf{F}_{IT}$ energy losses due to tidal conversion. The former is represented by the standard quadratic law:

$$\mathbf{F}_B = C_d \mathbf{u}|\mathbf{u}| \tag{3}$$

where $C_d = 0.003$ is a drag coefficient, and $\mathbf{u}$ tidal velocity. The conversion is written as $\mathbf{F}_{IT} = C_{IT}\mathbf{U}$, with the conversion coefficient C_{IT} given by (Green & Nycander, 2013; Zaron & Egbert, 2006)

$$C_{IT}(x,y) = \gamma \frac{(\nabla H)^2 N_b \overline{N}}{8\pi\omega} \tag{4}$$

where $\gamma = 50$ is a scaling factor (see Zaron & Egbert, 2006, for more details), N_b the buoyancy frequency at the sea-bed, $\overline{N}$ the vertical average of the buoyancy frequency, and ω is the frequency of the tidal constituent under evaluation. The buoyancy frequency is computed from a statistical fit based on observations from present day Earth, or $N(x,y) = 0.00524\exp(-z/1300)$, where z is the vertical coordinate, and the constants 0.00524 and 1,300 have units of s^{-1} and m, respectively. Whilst the abyssal stratification is known from the climate model simulations (see Section 2.3), the tides are relatively insensitive to changes in stratification within a factor 2 (Egbert et al., 2004). Furthermore, iterative studies, where stratification has been implemented in the tidal model

and the resulting dissipation returned to a climate model, showed only minor impact on the results (Schmittner et al., 2015).

2.2. Simulations and Computations

The tidal dissipation rates, D, were computed using the energy balance method (Egbert & Ray, 2001)

$$D = W - \nabla \cdot \mathbf{P} \tag{5}$$

The work rate done by the tide-generating force, W, and the energy flux, $\mathbf{P}$, are given by

$$W = g\rho_0 \langle \mathbf{U} \cdot \nabla(\eta_{eq} + \eta_{SAL}) \rangle \tag{6}$$

$$\mathbf{P} = g\rho_0 \langle \mathbf{U}\eta \rangle \tag{7}$$

in which $\langle\rangle$ denote time-averages over a tidal period. As the end result of tidal energy dissipation is heat, we add the tidal dissipation as tidal heating in the climate model.

Tidal model simulations were done for three rotation rates—12, 18, and 24 hr—using one topography—denoted "225"—from Blackledge et al. (2020). This was chosen because it consists of a series of smaller continents scattered around the planet, much like early Earth has been proposed to have looked like (Cawood et al., 2022; Hawkesworth et al., 2020; Sawada, 2020). The associated changes in tidal forcing due the closer proximity of the Moon for each investigated rotation rate was taken from Daher et al. (2021). The resulting tidal energy dissipation fields are shown in Figure 1.

2.3. Modeling Tidal Impacts on Early Earth's Climate

To investigate the impact of tidal energetics on the climate on early Earth, we employ the deep-time version of the intermediate-complexity climate model CLIMBER-3α (Montoya et al., 2005). The model is based on a modified version of the ocean general circulation model MOM3 (Hofmann & Morales Maqueda, 2006; Pacanowski & Griffies, 1999) run at a horizontal resolution of $3.75° \times 3.75°$ and using 24 levels vertically, a sea-ice model capturing both thermodynamics and dynamics (Fichefet & Morales Maqueda, 1997) at the same horizontal resolution as the ocean model, and a fast statistical-dynamical atmosphere model (Petoukhov et al., 2000) with a coarse horizontal resolution of 22.5° in longitude and 7.5° in latitude. The deep-time version of CLIMBER-3α entails the removal of parameterizations relating to the present-day climate system, additional diagnostics, and bug fixes. This version has been used in a range of studies relating to planetary habitability, in particular for the climate on early Earth (Kienert et al., 2012, 2013) and major glaciations in Earth's history (Eberhard et al., 2023; Feulner, 2017; Feulner & Kienert, 2014; Feulner et al., 2015, 2023).

All climate model simulations are run for the continental configuration "225" from Blackledge et al. (2020) as described above, re-gridded to the resolution of the ocean model (see Figure 2). The solar constant values corresponding to the three tidal scenarios with 12, 18, and 24 hr rotation rate are computed based on the relation between day length and time from Farhat et al. (2022) and the stellar evolution model MESA (Jermyn et al., 2023). For each rotation rate, simulations with three different atmospheric CO_2 levels are performed which are characterized by a low, medium, and high fraction of global sea-ice cover (see Table 1). We run four sets of nine simulations each:

1. *Control simulations* for the three tidal scenarios and three climate states without any tidal effects and ignoring geothermal heat flow. Key ocean and sea-ice characteristics of these simulations are shown in Figure B1 in Appendix B.
2. Same as 1., but including the effects of *tidal heating*. In this case, the energy input by the tides (computed as described in Sections 2.1 and 2.2, and shown in Figure 1) is implemented as additional bottom heat flux into the ocean.
3. Same as 2., but taking the *effects of tides on vertical mixing* into account. The vertical diffusivity is represented in the model by a constant background diffusivity, `afkph`, and an amplitude of the spatially varying diffusivity, `dfkph`. In the control simulations these are tuned to present day values of 0.8×10^{-4} and $1.05 \times 10^{-4}\,m^2\,s^{-1}$, respectively. At present day the energy required to sustain abyssal diffusivities is

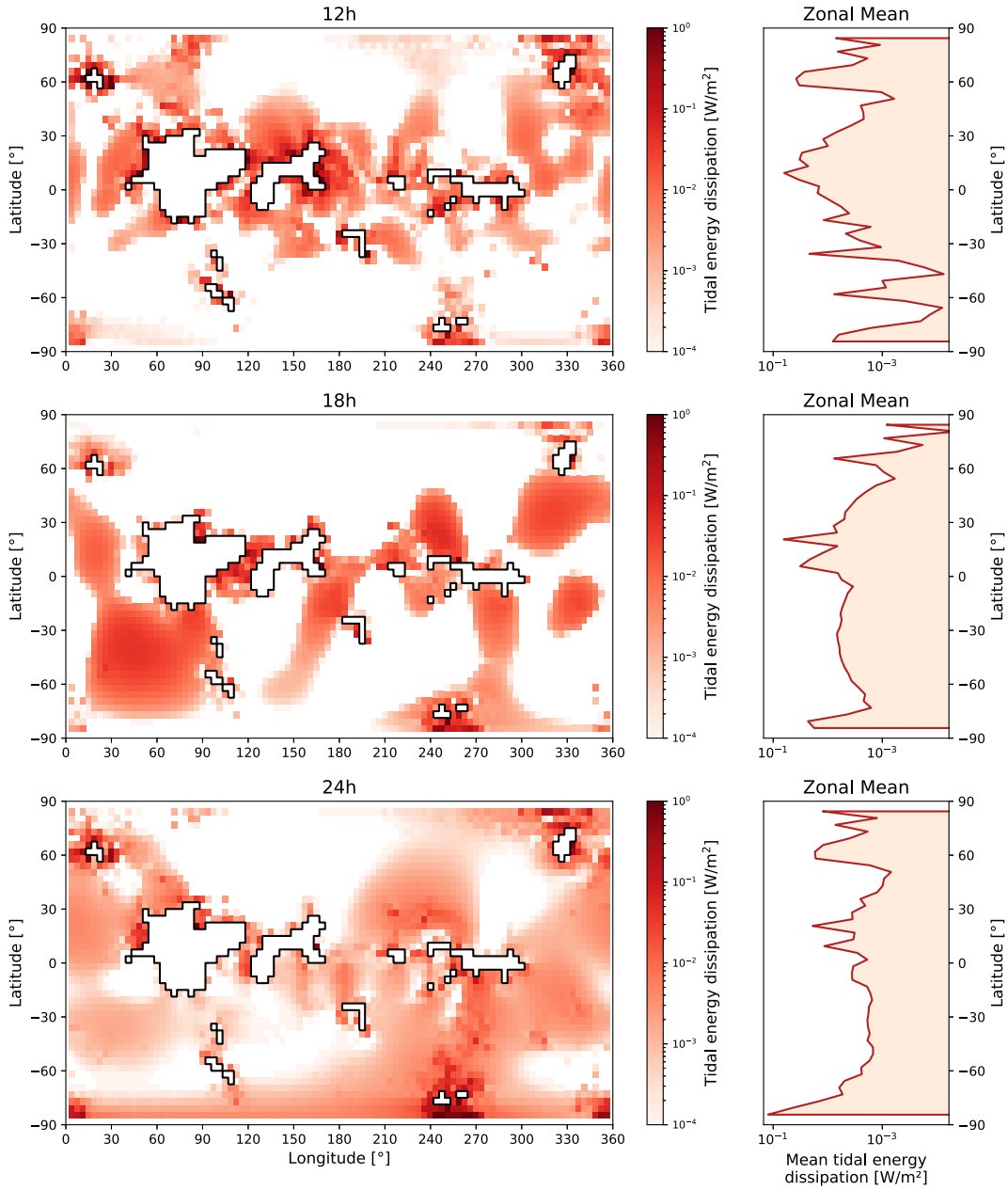

Figure 1. Maps (left column) and zonal means (right column) of modeled tidal dissipation rates for all three rotation rates of 12 hr (top panels), 18 hr (middle panels), and 24 hr (bottom panels). Note the logarithmic scale.

provided in equal parts by the wind and the tide (Wunsch & Ferrari, 2004), and we assumed the same ratio here. For simplicity, we computed the ratio, R, of the globally integrated abyssal tidal dissipation rates (i.e., in waters deeper than 500 m) from the simulations presented here to a present-day tidal model simulation (Green et al., 2017), that is, $R = D_{\text{Archaean}}/D_{\text{PD}}$. We then modify the tidally driven half of the `afkph` and `dfkph` by multiplying the control value with R so that `afkph` $= 0.8 \times (0.5 + 0.5R)$ and `dfkph` $= 1.05 \times (0.5 + 0.5R)$. The resulting values are shown in Table 2 and further highlight the existing knowledge that tidal dissipation rates, and hence vertical mixing, are to first order controlled by continental configuration (Blackledge et al., 2020; Green et al., 2018). The dissipation and associated diffusivity change by around 20% when we move from a present day topography (24 hr control) to our chosen Archean one (24 hr Archean). The reason for this is tidal resonances developing over large areas in the Archean topography. As we then change rotation rate, the Archean basins go out of resonances for an 18 hr day length; coincidentally the

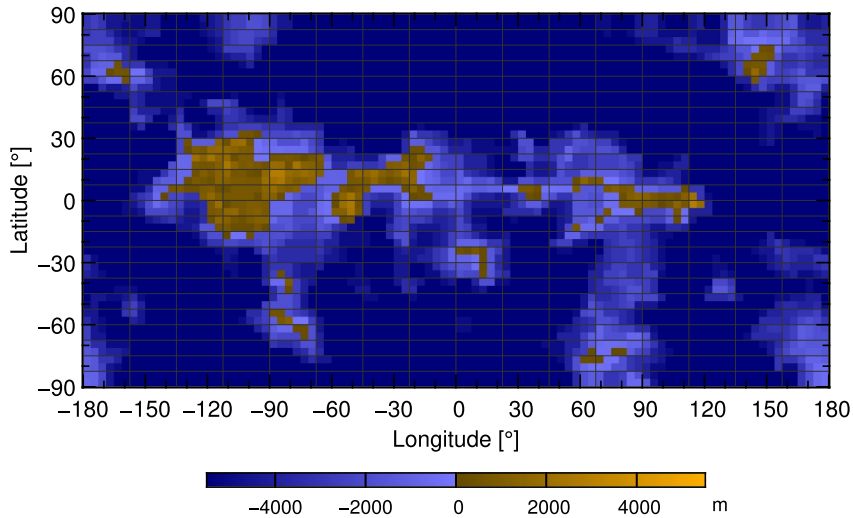

Figure 2. Ocean bathymetry and land orography based on continental configuration "225" from Blackledge et al. (2020) at the 3.75° × 3.75° resolution of CLIMBER-3α's ocean model.

background diffusivity is then the same as for present day. At 12 hr, the tides become more energetic and the diffusivity is 80% higher than at present. Note that Farhat et al. (2022) propose a rapid change in day length between 12 and 15 hr due to potential orbital resonances and our results support this. Also note that because the diffusivity is computed in waters deeper than 500 m and the tidal heating s the total dissipation, including shallow waters we can have the same total dissipation but different diffusivities and vice versa.

4. Same as 3., but *adding geothermal heat flux*. Time evolution of global geothermal heat flux from radioactive decay follows Turcotte and Schubert (2002), with the surface heat flow due to mantle cooling adjusted to 29 mW/m^2 to yield a present-day flux of 87 mW/m^2 for the modern continental configuration (Pollack et al., 1993). Furthermore, values are multiplied by a factor of 1.03 to take the partitioning between continental and oceanic crust for the lower total land area of continental configuration "225" into account. As for tidal heating, geothermal heat flux is uniformly distributed over the globe and added to the lowermost ocean cells; input to land areas is ignored in the model.

We employ an idealized present day-like orbital configuration with an obliquity of 23.5° and a circular orbit. All climate model simulations were integrated for at least 4,000 years until equilibrium was approached. Annual and global mean surface air and sea surface temperatures for all simulations can be found in Table A1 in Appendix A.

Table 1
Overview of Tidal Scenarios and Climate Model Simulations

Day length [hr]	Time [Myr]	Age [Ma]	S_0[W/m^2]	Tidal heating [mW/m^2]	Geothermal [mW/m^2]	CO_2 [ppm]	Ice cover [%]
12	867	3,700	1,010	14.40	217.7	176,000	16
						200,000	7.1
						220,000	3.0
18	2,767	1,800	1,161	10.90	121.6	15,000	15
						25,000	5.4
						28,000	3.2
24	4,567	0	1,361	2.758	90.42	140	14
						277	7.2
						350	4.5

Note. Tidal simulations are performed for three different day lengths; the corresponding point in time is estimated from day length following Farhat et al. (2022), the value of the solar constant S_0 at these times are obtained from stellar evolution model MESA (Jermyn et al., 2023). The corresponding global mean values for tidal heating (from the tidal model) and geothermal heating (see text for details) are indicated as well. For each of the three tidal scenarios, climate model simulations are performed at three atmospheric CO_2 concentrations for which the climate model simulations yield low, intermediate, and high global sea-ice cover.

Table 2
Summary of the Background (`afkph`) and Amplitude (`dfkph`) of the Vertical Diffusivities Used in the Simulations; the 24 hr Values Are the Present-Day Default Values Used in the Coupled Climate Model

Day length [hr]	afkph $[10^{-4}\ m^2\ s^{-1}]$	dfkph $[10^{-4}\ m^2\ s^{-1}]$
12, Archean	1.44	1.90
18, Archean	0.80	1.05
24, Archean	0.96	1.26
24, control	0.80	1.05

Note that rotation rates in the climate model simulations are 24 hr throughout to isolate the effect of tidal dissipation on the climate from the changes in Earth-system dynamics due to higher rotation rates (which are beyond the scope of this paper).

3. Results

In the following, we will look at the impact of tidal heating, tidal mixing, and geothermal heat flux on the climate for the different sets of simulations described in Section 2.3 by comparing the changes in key climate variables, in particular surface air temperature (SAT), sea-surface temperature (SST), sea-ice cover, and ocean surface velocities compared to the respective control simulations (the latter are shown in Figure B1). All diagnostics have been averaged over the last 500 years of each simulation to minimize the impact of inter-annual to centennial climate variability. With respect to the overall climate state, the global and annual mean SATs and SSTs of all simulations are summarized in Table A1. We structure the discussion of results of our simulation experiments following three key messages summarizing the dependence on rotation rate (Section 3.1, Figure 3), climate state (Section 3.2, Figure 4), and forcing (Section 3.3, Figures 5 and 6).

3.1. Climate Response to Tidal Heating Depends on Rotation Rate

For a given continental configuration, tidal dissipation (and thus heating) strongly depends on the assumed daylength (see Figure 1). These differences in tidal dissipation are also reflected in the climate response to this heating shown in Figure 3 for the intermediate climate state (the corresponding maps for all climate states can be found in Figure B2 in Appendix B). Although the global effect of tidal heating on the climate is very small (with global annual mean surface air temperature changes typically less than 0.1°C, see Table A1), marked regional impacts are visible at higher latitudes, varying with the spatial distribution and magnitude of tidal heating for different rotation rates.

These changes in sea-surface temperature, sea-ice cover, and ocean surface velocities in Figure 3 are largest close to the sea-ice edge and suggest that the response is (at least partly) mediated through changes in ocean currents. In our simulations, tidal heating impacts regional SST mostly by altering ocean surface currents and hence sea-ice dynamics as well as meridional heat transport. Depending on the patterns of the ocean surface currents and the sea-ice extent, tidal heating can have varying regional impacts. In particular, it is important to note that patterns of tidal heating do not necessarily correlate with regions of surface warming, as the tidal heat itself is too weak to penetrate to the surface and cause substantial changes in sea-ice cover (see below). Instead, the heating leads to changes in ocean surface currents which can trigger retreat or even advance of sea ice and thus local warming or cooling, respectively.

3.2. Climate Response to Tidal Heating Depends on Background Climate

The observation from Section 3.1 that tidal heating has the most significant effect on the climate if it can influence the sea-ice edge also leads to a strong dependence of the response to the background climate state, see Figure 4 for a rotation rate of 12 hr, and Figure B2 for all rotation rates and climate states.

Cold climate states with a large sea-ice extent experience hardly any impact of tidal heating on the ice cover. This is not too surprising, because the minute tidal warming mostly occurs at depth (see also Figure 7a), and because the extended sea-ice cover impedes strong meridional surface currents and heat exchange between the ocean and the atmosphere in the polar regions. Instead sea-ice cover reaches down to latitudes of roughly 50°N/S, respectively, where ocean surface currents are mostly zonal for the continental configuration used in our study (see Figure B1 in Appendix B) and thus do not greatly contribute to meridional heat transport toward the sea-ice edge.

Intermediate and warm climate states, on the other hand, show more pronounced impacts of tidal heating on sea-ice cover, as tidal heating influences ocean surface currents close to the sea-ice edge in this case, leading to changes in sea-ice cover and thus local climate, amplified by the ice-albedo feedback. Despite the fact that tidal heating is a source of energy to the ocean, the effects on SST and sea-ice extent by tidal heating can lead to either

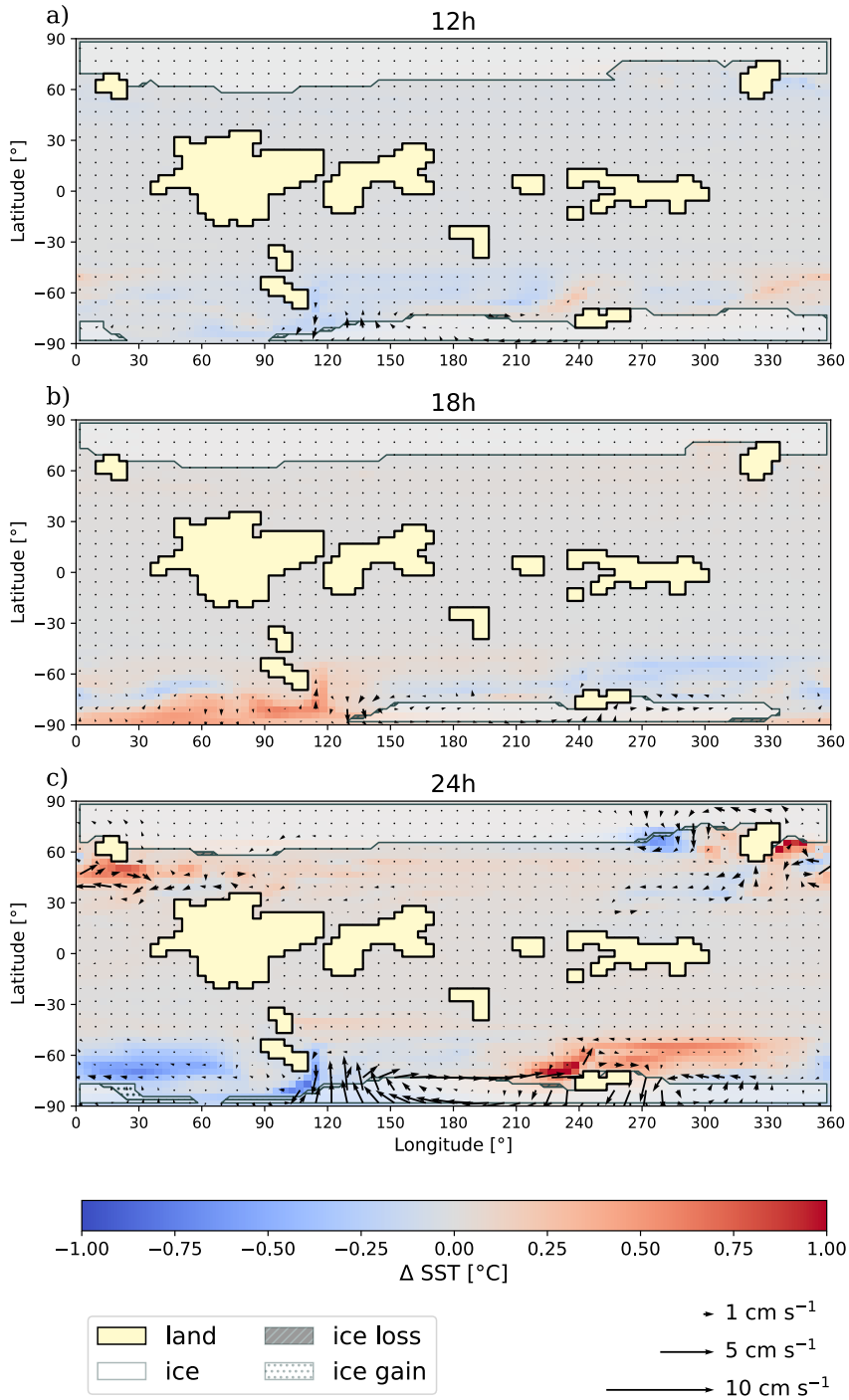

Figure 3. Tidal heating and climate-system response depend on rotation rate. Changes in sea-surface temperature, surface velocity, and sea-ice cover due to tidal heating for three different tidal scenarios with (a) 12 hr, (b) 18 hr, and (c) 24 hr rotation rate and for intermediate CO_2 levels. The blue and red colors correspond to changes in SST when introducing tidal heating. Yellow areas are land; semi-transparent white areas correspond to regions that have at least 50% sea-ice fraction in the annual mean. Dotted and hatched areas represent regions of sea-ice gain or loss, respectively. Arrows indicate a change in ocean surface currents, with their length scaling with the change in speed. Maps showing the effects of tidal heating for all climate states and all rotation rates can be found in Figure B2 in Appendix B.

regional warming or cooling depending on how ocean surface currents are affected. This also strongly depends on the continental configuration, of course. For example, the shape, position, and orientation of the islands at high southern latitudes leads to flow of warmer surface waters toward the polar region, significantly affecting local sea-

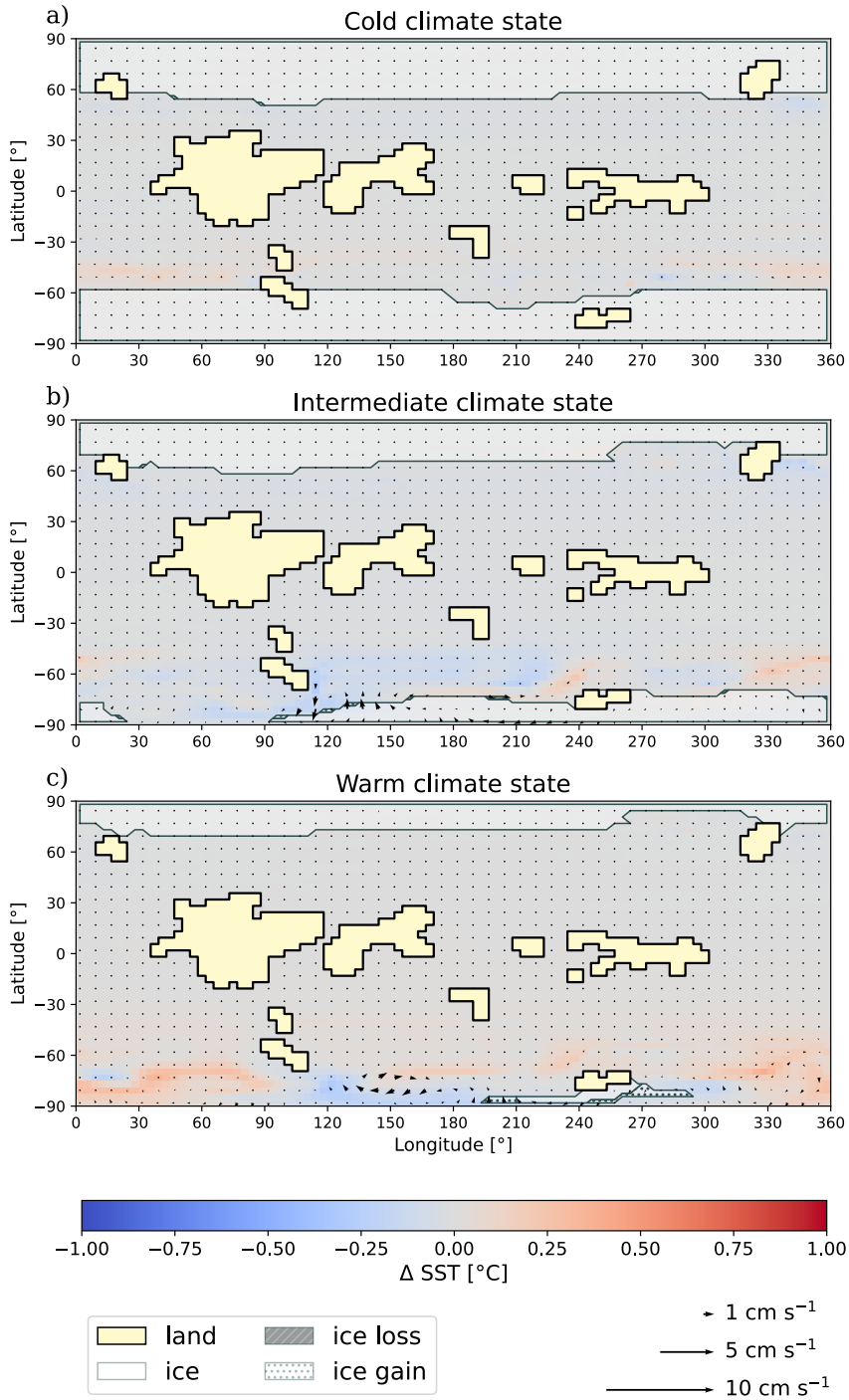

Figure 4. Response to tidal heating depends on background climate state. Changes in sea-surface temperature, surface velocity, and sea-ice cover due to tidal heating for a (a) cold, (b) intermediate, and (c) warm climate state and for a rotation rate of 12 hr. See caption of Figure 3 for explanation of colors and shading. Maps showing the effects of tidal heating for all rotation rates can be found in Figure B2 in Appendix B.

ice cover. The distribution of continents is also responsible for the North-South asymmetry in the response to tidal heating: There is slightly more land in the Southern hemisphere leading to an enhanced dissipation and tidal heating closer to the ocean surface (see Figure 7a) and to an offset in the global overturning circulation (see Figure 8a). It is therefore worth noting that even a small asymmetry in continental configuration can lead to

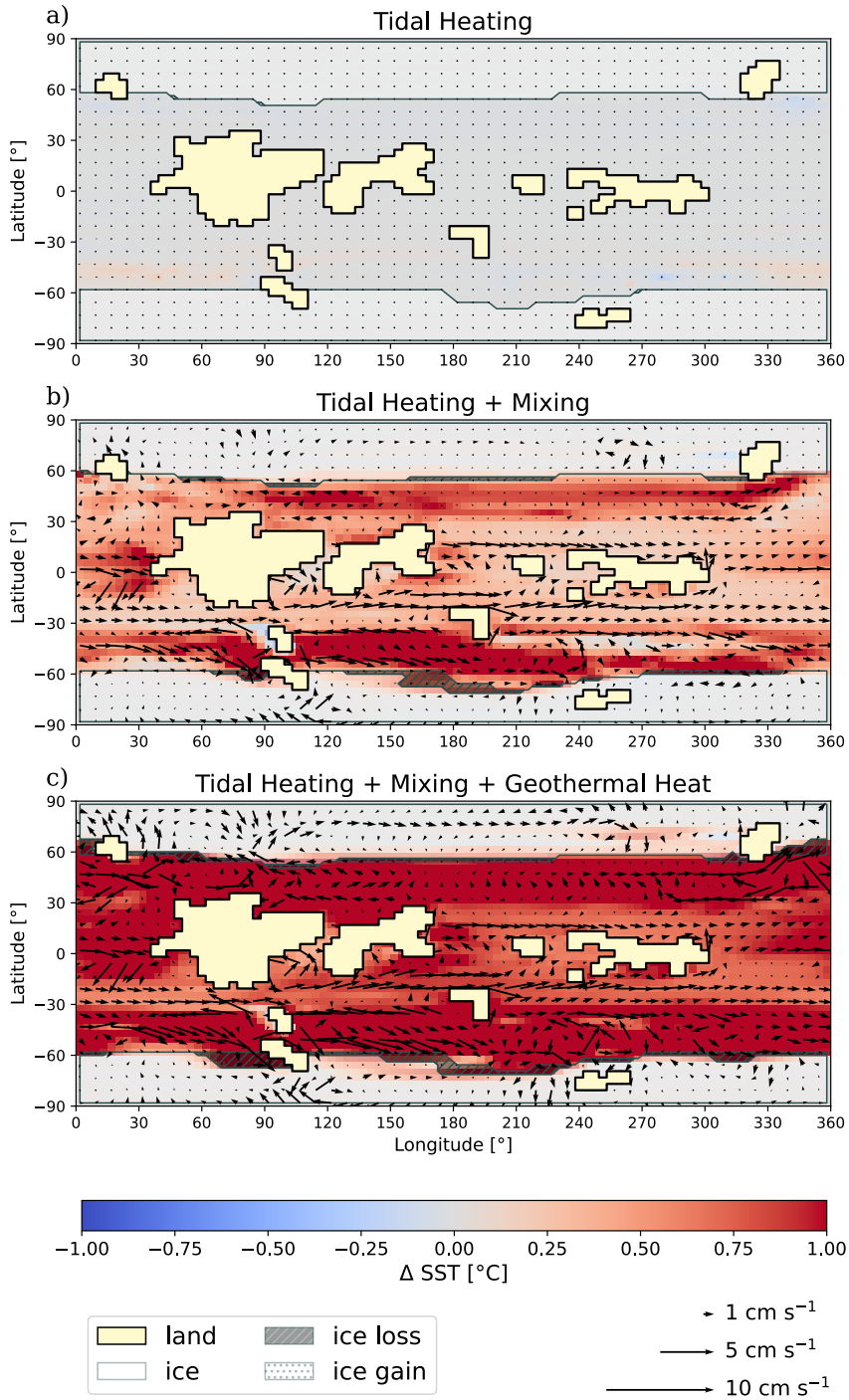

Figure 5. Tidal mixing and geothermal heat flow are more important than tidal heating (cold climate state). Changes in sea-surface temperature, surface velocity, and sea-ice cover for a cold climate state with 12 hr rotation rate and due to (a) tidal heating only, (b) tidal heating and mixing, and (c) tidal heating, mixing, and geothermal heat flow. See caption of Figure 3 for explanation of colors and shading. Appendix B contains all maps showing the effects of tidal heating (Figure B2), tidal heating and mixing (Figure B3), and tidal heating, mixing, and geothermal heat flux (Figure B4), respectively.

significant differences in the state of the ocean. In general, climate states with strong meridional surface currents near the sea-ice edge are more vulnerable to changes in ocean circulation. The impact of tidal heating is therefore strongest in these cases.

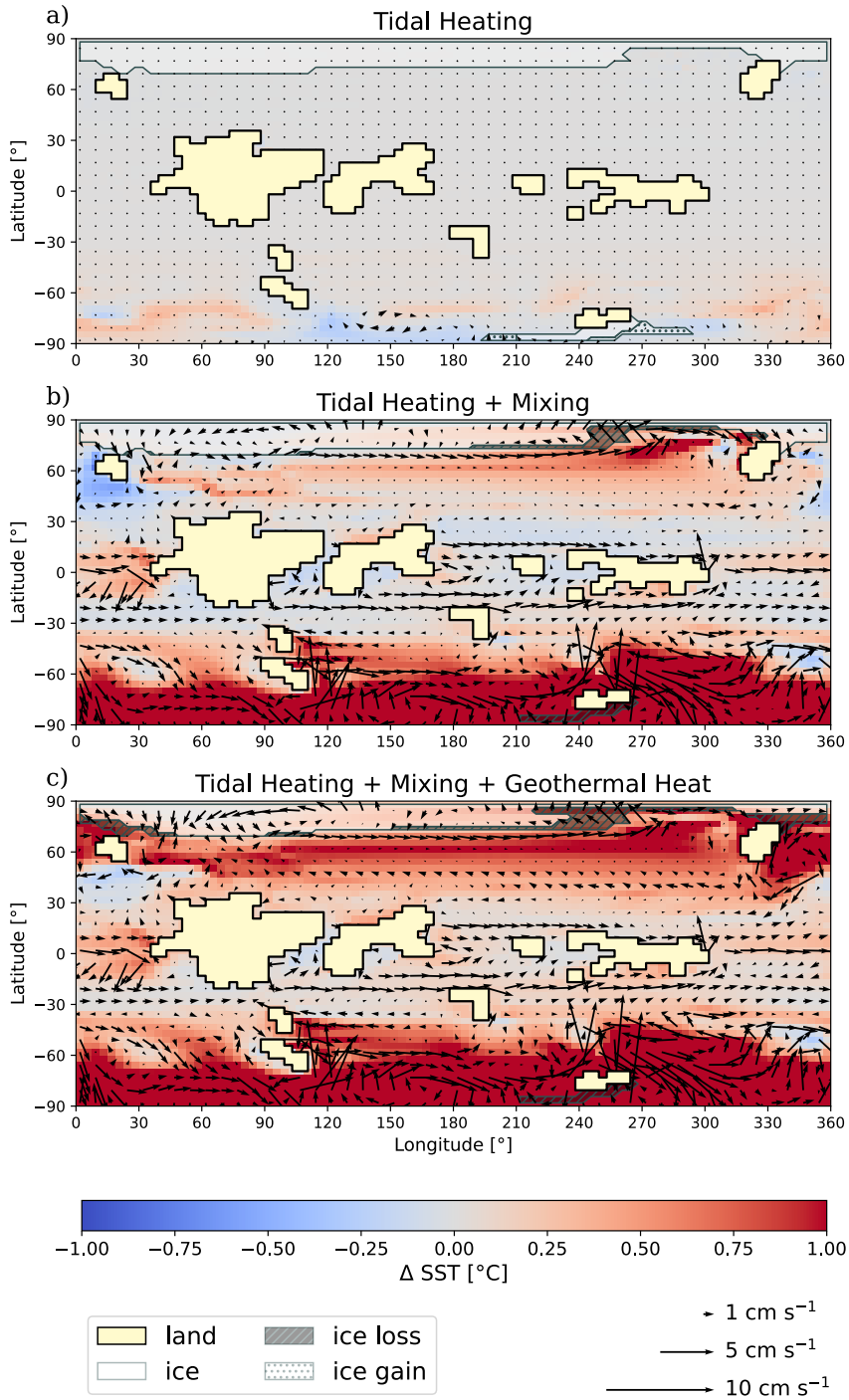

Figure 6. Tidal mixing and geothermal heat flow are more important than tidal heating (warm climate state). Same as Figure 5 but for a warm climate state. Appendix B contains all maps showing the effects of tidal heating (Figure B2), tidal heating and mixing (Figure B3), and tidal heating, mixing, and geothermal heat flux (Figure B4), respectively.

3.3. Tidal Mixing and Geothermal Heat Are More Important Than Tidal Heating

Despite the regional variations described above, the global impact of tidal heating on surface air temperatures, SSTs, and sea-ice cover is almost negligible, at least for the investigated continental configuration, tidal scenarios, and climate states. Tidally induced changes in global mean surface air temperatures vary between −0.022°C and +0.035°C, depending on tidal scenario and baseline state (for comparison, the standard deviation of the global

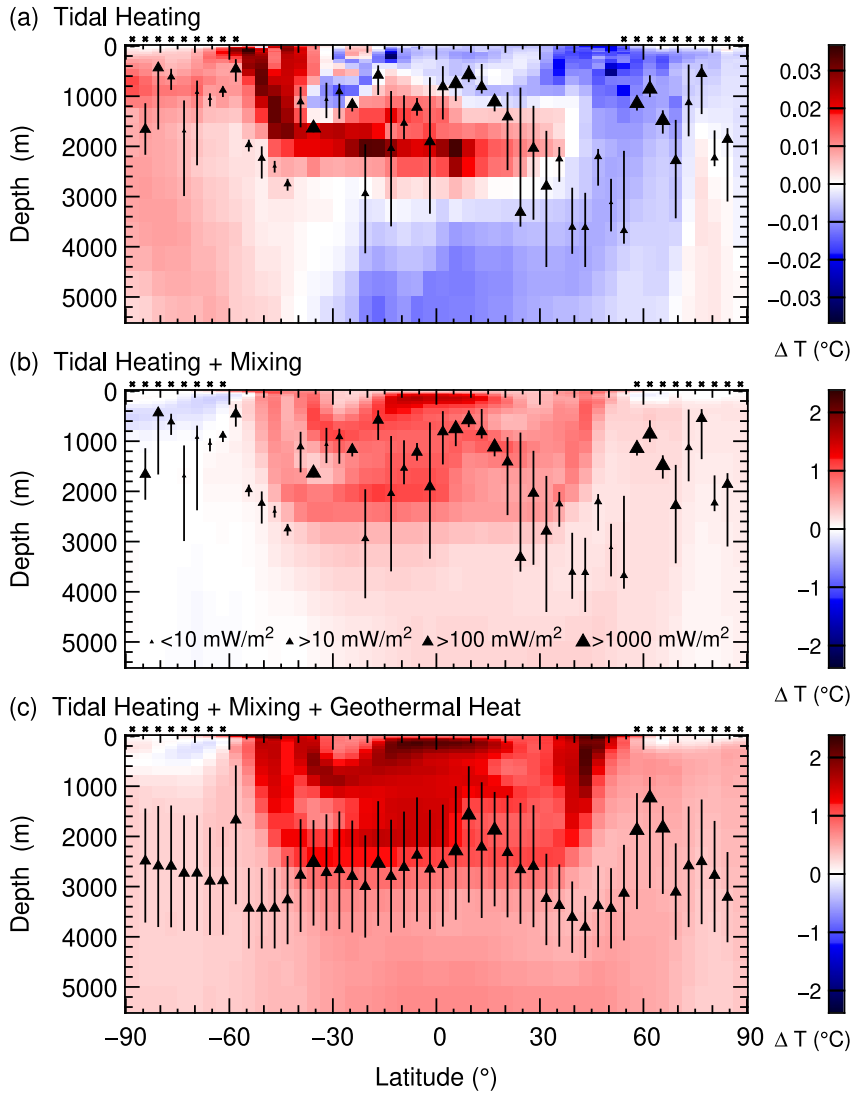

Figure 7. Depth-latitude section of potential temperature changes compared to the control simulation for a cold climate state and (a) tidal heating, (b) tidal heating plus mixing, and (c) tidal heating plus mixing plus geothermal heat flux. This corresponds to the results shown in Figure 5. Note the much smaller temperature changes for just tidal heating in panel (a). Asterisks at the ocean surface indicate areas of at least 50% annual-mean sea-ice cover. The filled triangles in panels (a) and (b) indicate the second quartile of the depth distribution of tidal heating, with the size of the symbol scaled according to the magnitude of maximum heating. The vertical lines indicate the first and third quartiles, respectively. The corresponding combined energy input from tidal heating and geothermal heat is indicated in a similar manner in panel (c).

mean temperature due to natural climate variability in the control simulations ranges from 0.003°C to 0.048°C). The mean difference in global sea-ice over all scenarios and states is about $+8.6 \times 10^4$ km^2 equivalent to a very small gain of 0.25% of the total sea-ice area.

As we have seen in Section 3.2, for a cold climate state and 12 hr rotation rate, for example, the influence of tidal heating is insignificant in the case of the cold climate state (Figures 4a and 5a) with the global and annual mean surface air temperature remaining the same as for the control simulation (9.2°C). The reason becomes obvious when looking at the temperature distribution with depth and latitude (Figure 7a). As the tidal heating is small (fractions of a W m^{-2}), the heat itself is not large enough to penetrate to the ocean surface and directly influence SSTs unless the energy input occurs close to the ocean surface. In some regions, the energy input from tidal heating leads to a small warming at depth, other regions show slight cooling due to changes in ocean circulation. In general, these temperature changes are small ($|\Delta T| < 0.05$°C) and cannot significantly affect the surface

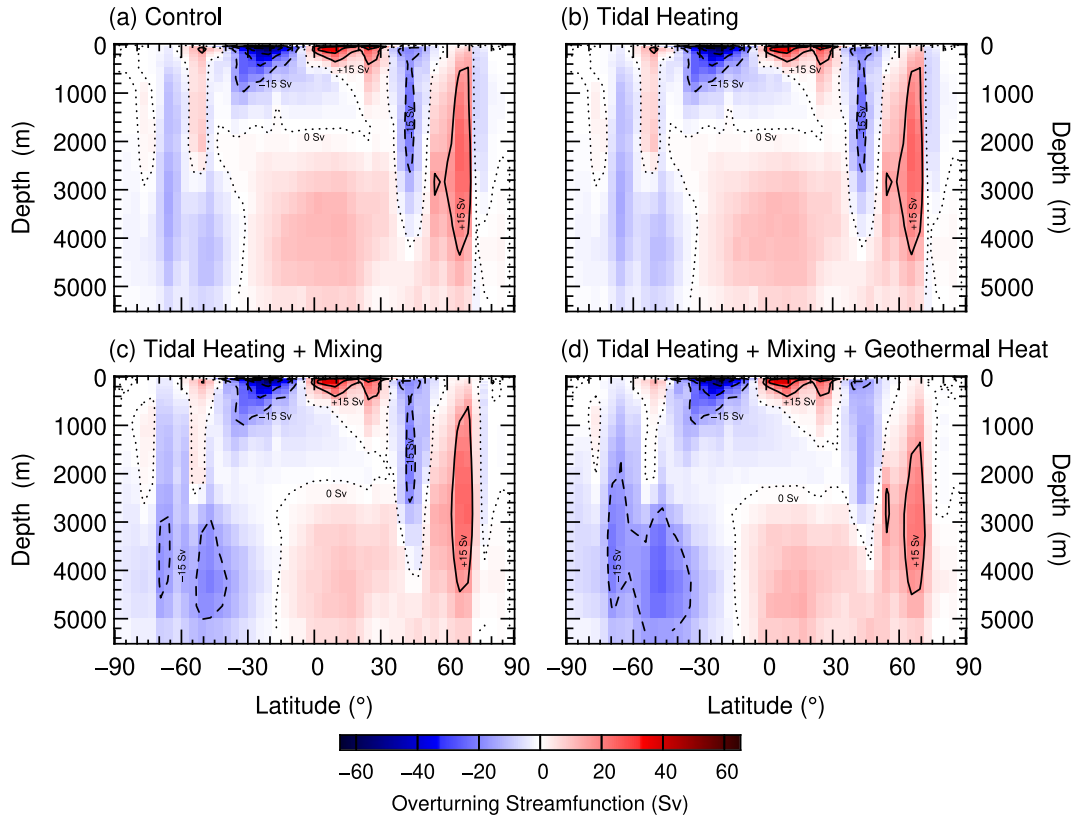

Figure 8. Global overturning streamfunction for a cold climate state with 12 hr rotation rate and (a) the control simulation, (b) tidal heating only, (c) tidal heating plus mixing, and (d) tidal heating, mixing, and geothermal heat flow (the simulations shown in Figures 5 and 7). Colors indicate the strength of the streamfunction. Contours are drawn in intervals of 15 Sv with negative values shown as dashed lines, the zero contour as dotted line, and positive values as solid lines.

climate. Furthermore, tidal heating does not significantly change the amplitude or structure of the global overturning (see Figures 8a and 8b).

The response of the climate to tides changes significantly when taking the effect of tidal mixing into account in addition to just tidal heating (see Figures 5b and 6b for the cold and warm climate state, respectively). In this case, the global climate is significantly warmer, with a global and annual mean surface air temperature of 10°C compared to 9.2°C in the control simulation for the cold climate state. Generally speaking, tidally enhanced ocean mixing will transport the tidal heat from the deeper ocean layers toward the surface and can thus affect the surface climate either directly or via changes in ocean currents or sea-ice cover, amplified by the ice-albedo feedback. This effect can clearly be seen in the depth-latitude temperature section (Figure 7b). For all climate states and rotation rates, the changes in global and annual mean surface air temperatures compared to the respective control simulations range from −0.013°C to +0.72°C when tidal mixing is included. Global sea-ice area changes by about $-3.8 \times 10^6\,\mathrm{km}^2$, equivalent to a loss of 11% of the total sea-ice area of the corresponding control simulation.

Adding geothermal heat flux on top of tidal heating and mixing leads to even more pronounced changes in the surface climate (see Figures 5c and 6c for the cold and warm climate state, respectively), with global mean surface air temperature changes relative to the control simulations in the range of +0.13°C to +1.7°C depending on the tidal scenario and climate state. The mean change in sea-ice area is also more substantial in this case, about $-6.9 \times 10^6\,\mathrm{km}^2$, equivalent to a loss of 19% of the total sea-ice area in the control simulations. The larger response is hardly surprising given that the geothermal heat flux is one order of magnitude larger than the tidal heating (see Table 1). For the cold climate case, for example, the global and annual mean surface air temperature

increases to 11°C, and thus 1.0°C higher than for the simulation with tidal heating plus mixing or 1.8°C higher than the control simulation. Compared to the simulation with tidal heating, the input of heat is more uniform and generally at larger depths, leading to an overall warming of the ocean on top of the changes induced by tidal heating and mixing (see Figure 7c).

The global overturning streamfunction (Figure 8) shows a northern hemisphere clockwise cell with a maximum of about 25 Sv between 60 and 70°N. This shows that deepwater forms in the north and spreads out at depth, much like in the present day North Atlantic. There is a corresponding counter-clockwise cell in the southern hemisphere, but it is much weaker than the cell in the north in the control and tidal heating runs (Figures 8a and 8b). As tidal mixing is included, the southern cell becomes more energetic, and with all tidal processes and geothermal heat switched on (Figure 8d) there is a deep cell in the southern hemisphere with a maximum of some 20 Sv between 30 and 70°S. It has been known for some time that the strength of the overturning circulation depends on the level of vertical mixing (e.g., Wunsch & Ferrari, 2004) and in this configuration, that leads to the establishment of the southern hemisphere cell.

Compared to the cold climate state (Figure 5), the effects get more pronounced for the warm climate state (Figure 6) as already discussed in Section 3.2 for the effects of tidal heating alone.

4. Discussion

To help resolve the FYSP through tidal heating, the tidal heating rate would be required to contribute significantly to Earth's energy balance. Based on global numbers, Archean tidal heating is generally considered to be too low to counteract the low solar input (Feulner, 2012), as even geothermal heat flux is greater by one order of magnitude. Although Heller et al. (2021) argue that tidal heating rates may be underestimated, they also conclude that tidal heating helped to maintain liquid surface water for the first 220 Myr of Earth's existence at most, and hence is most important during the Hadean rather than the Archean.

Our spatially-resolved simulations of tidal dissipation and its impact on climate confirm that the tidal heat itself does not contribute to a measurable increase in the surface energy budget. Instead, tidal heating induces local changes in ocean currents and thus sea-ice dynamics and meridional heat transport. These secondary effects then may lead to regional cooling or warming of the ocean surface and associated changes in sea-ice cover, which amplify the changes in temperature via the ice-albedo feedback. On the other hand, our results also indicate that a large ice extent makes the climate more robust against impacts from tidal heating due to the insulating effect of sea-ice cover. Furthermore, the impact of tidal heating on the global climate on early Earth is negligible.

However, including the effect of tidal dissipation on vertical mixing in the ocean leads to more pronounced warming. Combined with the heating from the higher geothermal heat flux on early Earth, tides can thus contribute to warming the climate under the faint young Sun.

Our approach of using a state-of-the-art tidal model and a coupled climate model to investigate the effects of tidal heating on early Earth's climate spatially resolved can certainly be considered an improvement compared to simple global assessments. Nevertheless, our study is just a first step toward a more complete assessment of the influence of tides on early Earth's climate, with a number of questions still to be investigated.

First, one key factor determining tidal dissipation is the distribution of landmasses, which is unknown for early Earth. The continental configuration used in this study is randomly generated due to the lack of knowledge about Hadean and Archean Earth. As the landmasses strongly influence both the magnitude of tidal heating and its potential impact on meridional currents, the results of our study allow an assessment only for this particular continental configuration. Systematic ensemble investigations of different random continental configurations may find that there are scenarios in which lunar tides have a stronger influence on Earth's climate compared to the configuration investigated above, considering that tidal dissipation can vary by three orders of magnitude for different land-ocean distributions (Blackledge et al., 2020) and that continental configuration can also significantly affect the snowball bifurcation point (Eberhard et al., 2023).

Second, the tides are not implemented dynamically, but the tidal dissipation fields are used to provide an additional heat source at the bottom of the ocean in the tidal heating runs and to drive vertical mixing in the mixing

runs. The change in the ocean temperature structure and overturning stream function as tidally driven mixing is implemented (Figures 7 and 8) show that using physically sound vertical mixing rates for the time period under consideration is necessary; present day mixing rates are poor proxy for past rates.

Third, despite the fact that the tidal heating and mixing are computed using a tidal model with day lengths of 12, 18, and 24 hr, our coupled climate model only simulates the climate dynamics of a present 24 hr length of day. Hence, any consequences of a faster rotation (e.g., the narrowing or appearance of additional atmospheric circulation cells) are not considered. Earlier work has shown that the snowball bifurcation is intricately linked to the large-scale circulation patterns in the atmosphere (Feulner et al., 2023). In this context it is important to note that there is still a large uncertainty in the evolution of Earth's day length which translates also into a larger uncertainty in the rate of tidal heating at our chosen points in time.

Finally, tides within Earth's mantle were dominant during the freezing of Earth's surface in the first million years of the Hadean (Zahnle et al., 2007). After the mantle became solid, oceanic tides probably were the key driver for tidal heating (Blackledge et al., 2020), and hence our study focuses on ocean tides. More recent research (Daher et al., 2021) also investigated the impact of atmospheric tides which may have helped to stabilize Earth's rotation, but the direct effect of these on the ocean would have been small. A more thorough investigation of tides in a magma ocean would be very interesting but is beyond our scope here.

5. Conclusions

In summary, our study uses spatially resolved maps of tidal dissipation from a state-of-the-art tidal model which represent more realistic tidal energy inputs compared to simple exponential models or the CPL model by Heller et al. (2021) that assume a globally uniform tidal heating. By forcing a coupled climate model with this spatially-resolved tidal heating, tidal mixing, and geothermal heat flux our study makes a step further toward understanding the impacts of tides onto the climate on early Earth and contributes to assessing what role tides could have played in context of the FYSP.

Our results show that the global effect of tidal heating is insignificant but that tidal heating can affect sea-ice cover on local and regional scales and account for a substantial change in sea ice cover. In some scenarios the fraction of ice covered area of a grid cell is altered by more than 20% due to the tidal heating. This impact is achieved by inducing changes in the ocean currents and thus in sea-ice dynamics as well as of heat transport toward the ice line. Tidal heating alone is thus certainly not the solution to the FYSP, as it does not provide enough energy. However, our results show that tidal heating can have regional impacts. The fact that tidal heating acts primarily via altering oceanic currents underlines the importance of dynamical features when investigating tidal impacts.

Out study also shows that tidal mixing and geothermal heat flux are much more important than tidal heating alone. In particular the effects of tidal mixing should be included in future studies of deep-time paleoclimate states. With respect to the effect of tides on the climate on early Earth, future studies will have to investigate the effects of a shorter day length on the dynamics of the coupled Earth system under the faint young Sun and subject to stronger tidal forcing.

Appendix A: Global Mean Temperatures for All Simulations

The global mean surface air and sea surface temperatures of all simulations are summarized in Table A1.

Table A1
Global and Annual Mean Surface Air Temperatures (SATs) and Sea-Surface Temperatures (SSTs) for All Simulations

S_0 [W/m^2]	CO_2 [ppm]	Simulation	SAT [°C]	SST [°C]
1,010	176,000	Control	9.23	12.0
		Tidal heating	9.22	12.0
		Tidal heating + mixing	9.95	12.4
		Tidal heating + mixing + geothermal	11.0	13.1
	200,000	Control	14.3	15.3
		Tidal heating	14.2	15.3
		Tidal heating + mixing	14.8	15.8
		Tidal heating + mixing + geothermal	15.0	16.0
	220,000	Control	16.7	17.2
		Tidal heating	16.7	17.2
		Tidal heating + mixing	17.0	17.4
		Tidal heating + mixing + geothermal	17.2	17.6
1,161	15,000	Control	10.7	13.4
		Tidal heating	10.7	13.4
		Tidal heating + mixing	10.8	13.4
		Tidal heating + mixing + geothermal	10.9	13.5
	25,000	Control	16.3	17.2
		Tidal heating	16.3	17.2
		Tidal heating + mixing	16.3	17.2
		Tidal heating + mixing + geothermal	16.5	17.3
	28,000	Control	17.5	18.0
		Tidal heating	17.5	18.0
		Tidal heating + mixing	17.5	18.0
		Tidal heating + mixing + geothermal	17.6	18.1
1,361	140	Control	11.8	14.8
		Tidal heating	11.8	14.8
		Tidal heating + mixing	11.9	14.8
		Tidal heating + mixing + geothermal	12.0	14.9
	277	Control	16.1	17.6
		Tidal heating	16.2	17.6
		Tidal heating + mixing	16.2	17.7
		Tidal heating + mixing + geothermal	16.3	17.7
	350	Control	17.7	18.7
		Tidal heating	17.7	18.7
		Tidal heating + mixing	18.0	18.9
		Tidal heating + mixing + geothermal	18.1	19.0

Note. All values are computed over the last 500 years of each simulation.

Appendix B: Additional Figures

Key ocean and sea-ice characteristics of the control simulations are shown in Figure B1, followed by maps showing the effects of tidal heating (Figure B2), tidal heating and mixing (Figure B3), and tidal heating, mixing, and geothermal heat flux (Figure B4), respectively.

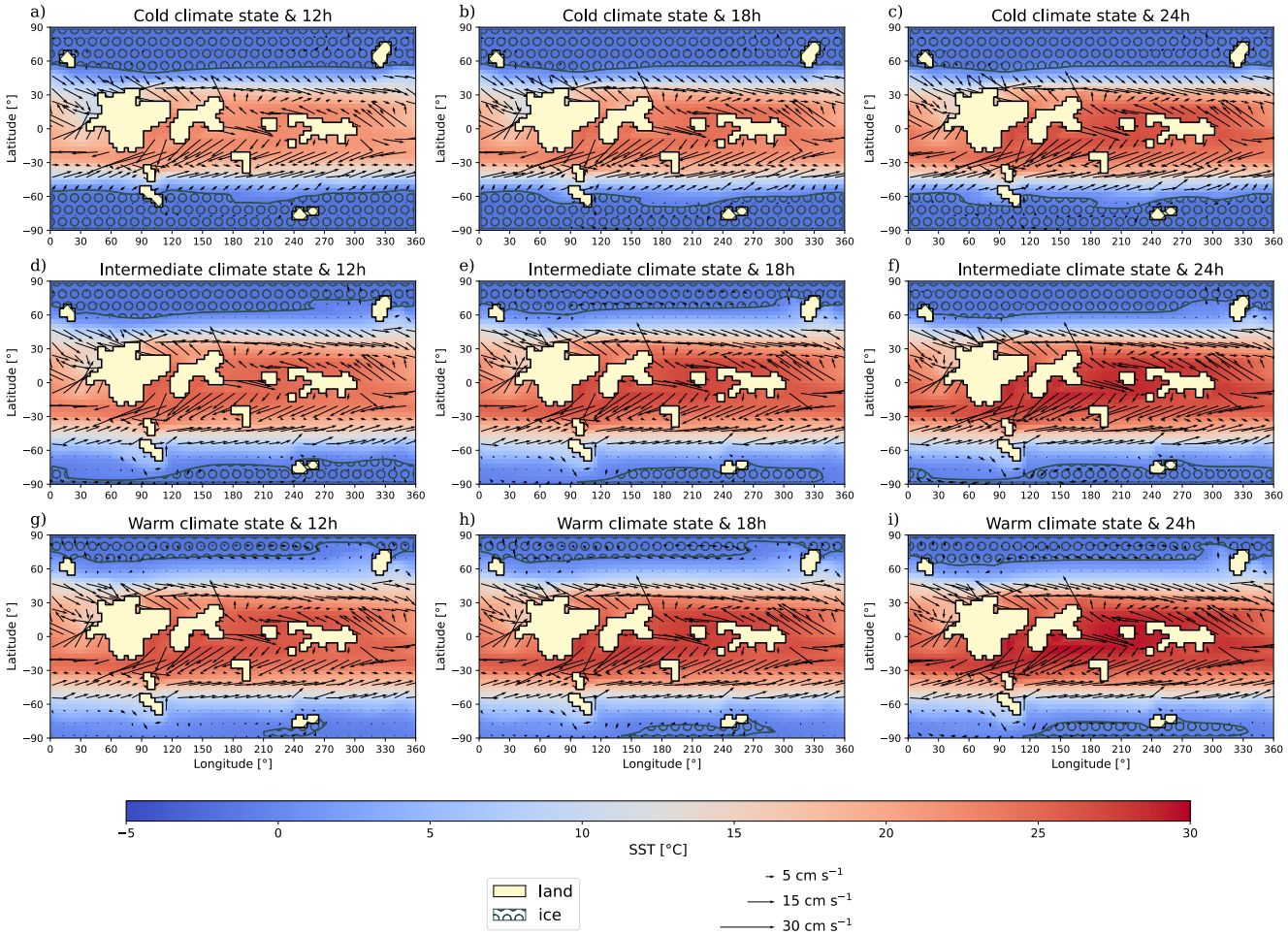

Figure B1. Control simulations. Absolute sea-surface temperatures (SSTs), surface velocities, and sea-ice cover (grid cells with annual-mean sea-ice fraction of at least 50%) for the nine control simulations without tides and geothermal heat flux.

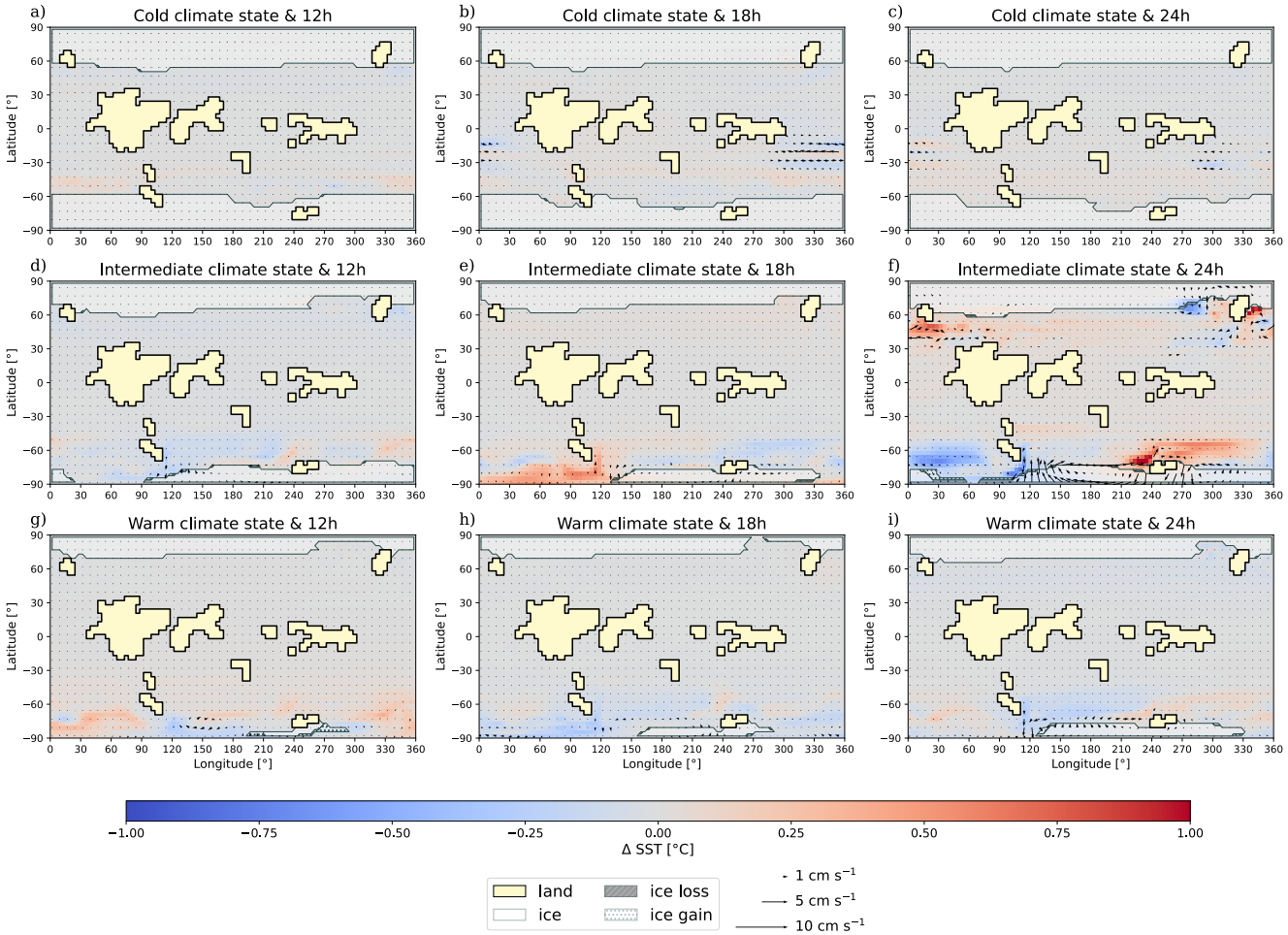

Figure B2. Simulations with tidal heating. Changes in sea-surface temperature, surface velocity, and sea-ice cover due to tidal heating for three different tidal scenarios with (a, d, g) 12 hr, (b, e, h) 18 hr, and (c, f, i) 24 hr rotation rate and for (a, b, c) low, (d, e, f) intermediate, and (g, h, i) high CO_2 levels corresponding to cold, intermediate, and warm climate states, respectively. The blue and red colors correspond to changes in SST when introducing tidal heating. Yellow areas are land; semi-transparent white areas correspond to regions that are covered have at least 50% sea-ice fraction in the annual mean. Dotted and hatched areas represent regions of sea-ice loss or gain, respectively. Arrows indicate a change in ocean surface currents, with their length scaling with the change in speed. Figure 3 corresponds to the panels in the second row, Figure 4 to the ones in the first column.

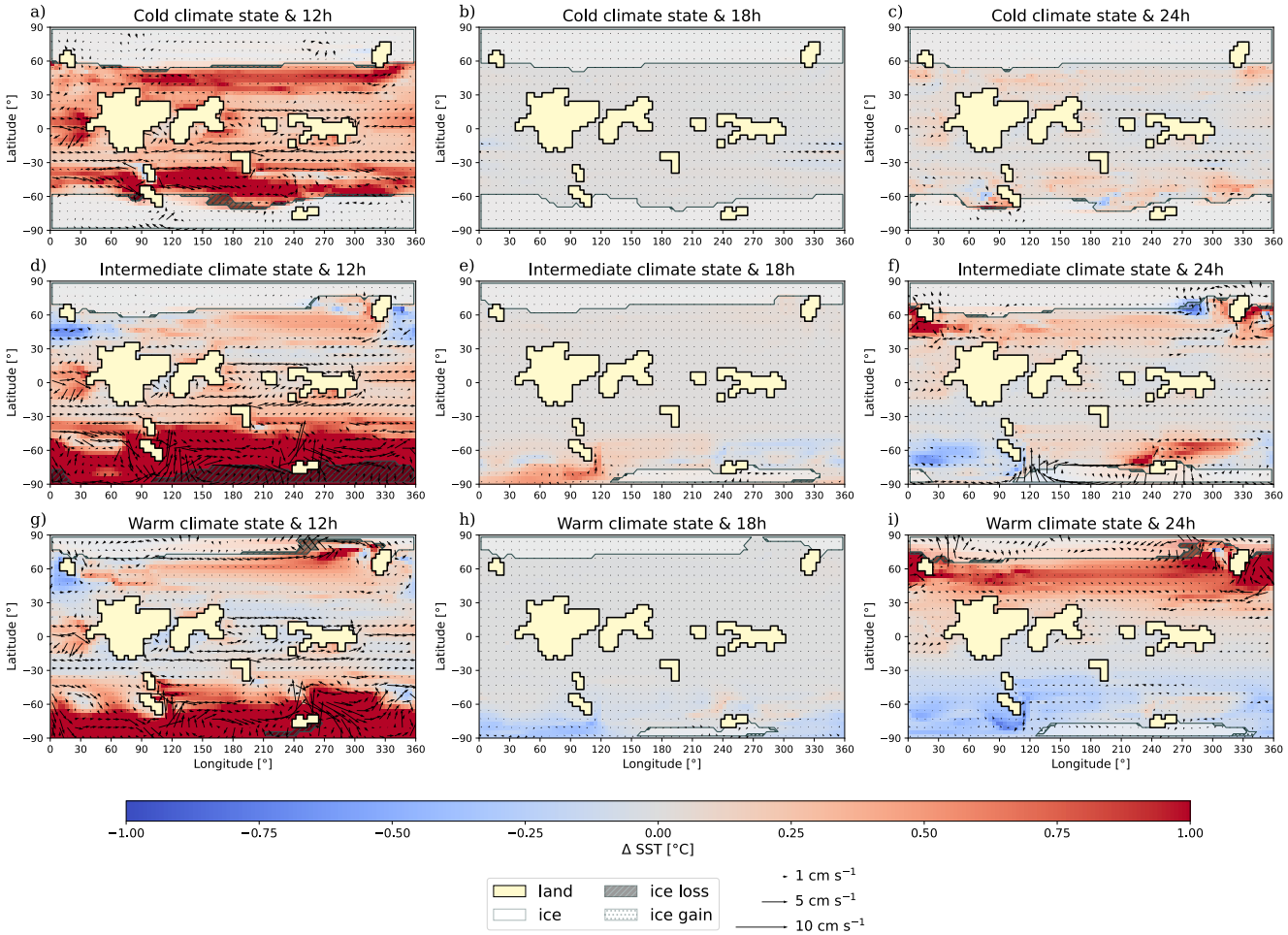

Figure B3. Simulations with tidal heating and mixing. Same as Figure B2 but for the simulations also including the effects of tidal mixing. Note that the mixing parameters for 18 hr daylength are the same as the default model parameters.

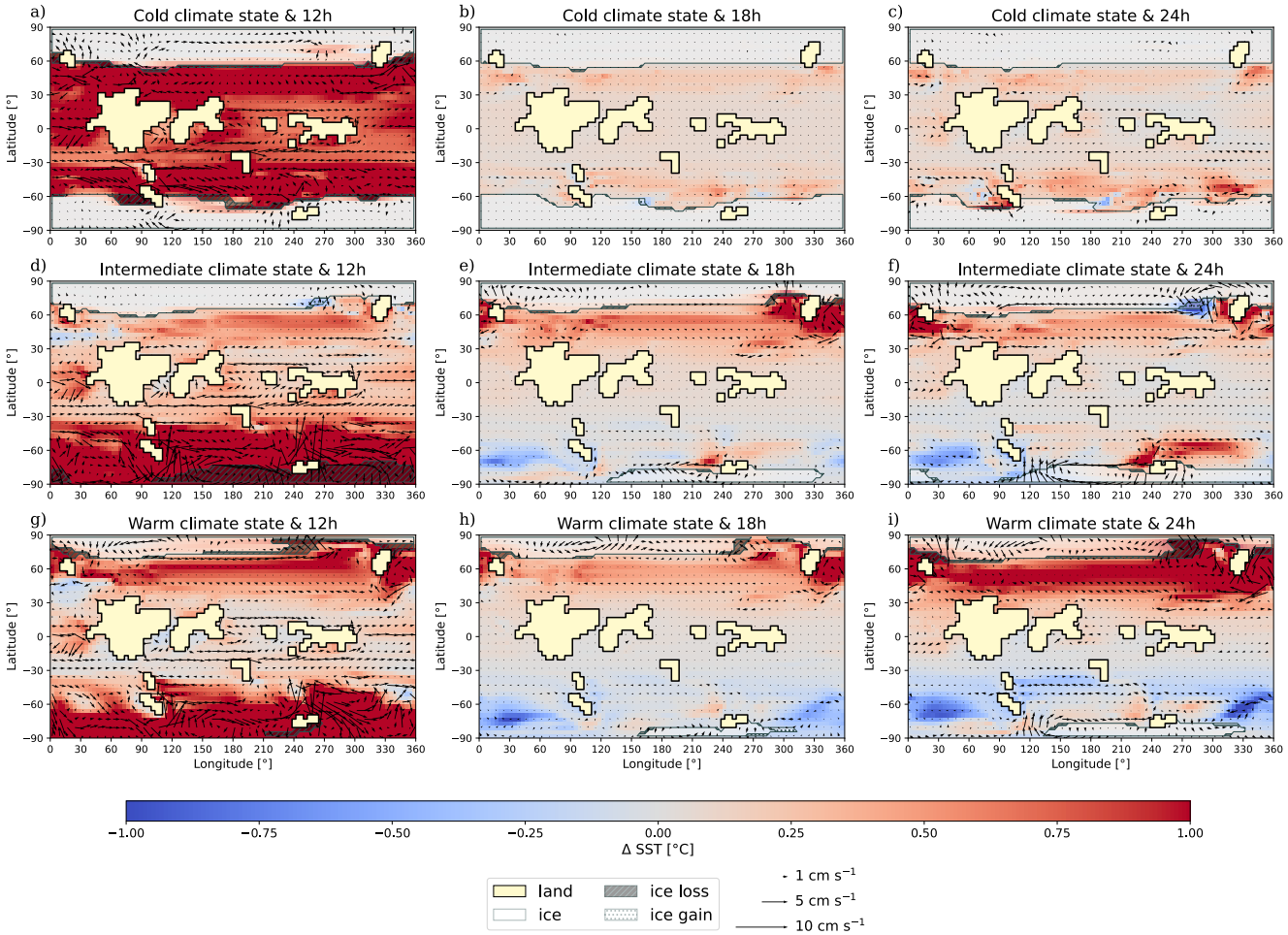

Figure B4. Simulations with tidal heating, mixing, and geothermal heat flux. Same as Figure B3 but for the simulations also including the effects of geothermal heat flux.

Acronyms

SST	Sea Surface Temperature
CLIMBER	CLIMate-BiosphERe Model
EMIC	Earth system Model of Intermediate Complexity
FYSP	Faint Young Sun Problem
GCM	General Circulation Model
AOGCM	Atmospheric-Oceanic General Circulation Model

Data Availability Statement

All model input and output files as well as the pre-processing and post-processing scripts used to generate model input and the figures in the paper are published via the GFZ data portal (Biewald et al., 2024). The source code for the model used in this study is archived at the Potsdam Institute for Climate Impact Research and is made available upon request to the corresponding authors.

Acknowledgments
The European Regional Development Fund (ERDF), the German Federal Ministry of Education and Research and the Land Brandenburg are gratefully acknowledged for supporting this project by providing resources on the high performance computer system at the Potsdam Institute for Climate Impact Research. JAMG acknowledges funding from The Leverhulme trust (Grant RPG-2021-091) and The Natural Environment Research Council (Grant NE/S009566/1). The tidal model simulations were done on Supercomputing Wales through Bangor University. The authors thank two anonymous reviewers and the editor, Matthew Huber, for their comments which helped improve the manuscript.

References

Balbus, S. A. (2014). Dynamical, biological and anthropic consequences of equal lunar and solar angular radii. *Proceedings of the Royal Society A: Mathematical, Physical and Engineering Sciences*, *470*(2168), 20140263. arXiv: 1406.0323. https://doi.org/10.1098/rspa.2014.0263

Barnes, R., Raymond, S. N., Jackson, B., & Greenberg, R. (2008). Tides and the evolution of planetary habitability. *Astrobiology*, *8*(3), 557–568. https://doi.org/10.1089/ast.2007.0204

Biewald, B., Feulner, G., Petri, S., Hofmann, M., & Green, M. (2024). Model data of the impacts of tidal energy dissipation on early Earth's climate. V. 2024-07-24 [Dataset]. *GFZ Data Services*. https://doi.org/10.5880/PIK.2023.004

Bills, B. G., & Ray, R. D. (1999). Lunar orbital evolution: A synthesis of recent results. *Geophysical Research Letters*, *26*(19), 3045–3048. https://doi.org/10.1029/1999gl008348

Blackledge, B., Green, M., Barnes, R., & Way, M. (2020). Tides on other earths: Implications for exoplanet and palaeo-tidal simulations. *Geophysical Research Letters*, *47*(12), e2019GL085746. https://doi.org/10.1029/2019GL085746

Byrne, H. M., Green, J. A., Balbus, S. A., & Ahlberg, P. E. (2020). Tides: A key environmental driver of osteichthyan evolution and the fish-tetrapod transition? *Proceedings of the Royal Society A: Mathematical, Physical and Engineering Sciences*, *476*(2242). https://doi.org/10.1098/rspa.2020.0355

Cawood, P. A., Chowdhury, P., Mulder, J. A., Hawkesworth, C. J., Capitanio, F. A., Gunawardana, P. M., & Nebel, O. (2022). Secular evolution of continents and the earth system. *Reviews of Geophysics*, *60*(4), e2022RG000789. https://doi.org/10.1029/2022RG000789

Daher, H., Arbic, B. K., Williams, J. G., Ansong, J. K., Boggs, D. H., Müller, M., et al. (2021). Long-term Earth-moon evolution with high-level orbit and ocean tide models. *Journal of Geophysical Research: Planets*, *126*(12), e2021JE006875. https://doi.org/10.1029/2021JE006875

Eberhard, J., Bevan, O. E., Feulner, G., Petri, S., van Hunen, J., & Baldini, J. U. L. (2023). Sensitivity of Neoproterozoic snowball-earth inceptions to continental configuration, orbital geometry, and volcanism. *Climate of the Past*, *19*(11), 2203–2235. https://doi.org/10.5194/cp-19-2203-2023

Egbert, G. D., Bills, B. G., & Ray, R. D. (2004). Numerical modeling of the global semidiurnal tide in the present day and in the last glacial maximum. *Journal of Geophysical Research*, *109*(C3), C03003. https://doi.org/10.1029/2003JC001973

Egbert, G. D., & Ray, R. D. (2001). Estimates of M2 tidal energy dissipation from Topex/Poseidon altimeter data. *Journal of Geophysical Research*, *106*(C10), 22475–22502. https://doi.org/10.1029/2000jc000699

Eulenfeld, T., & Heubeck, C. (2023). Constraints on Moon's orbit 3.2 billion years ago from tidal bundle data. *Journal of Geophysical Research*, *128*(1), e2022JE007466. https://doi.org/10.1029/2022JE007466

Farhat, M., Auclair-Desrotour, P., Boué, G., & Laskar, J. (2022). The resonant tidal evolution of the Earth-Moon distance. *Astronomy & Astrophysics*, *665*, L1. https://doi.org/10.1051/0004-6361/202243445

Feulner, G. (2012). The faint young sun problem. *Reviews of Geophysics*, *50*(2), RG2006. https://doi.org/10.1029/2011RG000375

Feulner, G. (2017). Formation of most of our coal brought Earth close to global glaciation. *Proceedings of the National Academy of Sciences*, *114*(43), 11333–11337. https://doi.org/10.1073/pnas.1712062114

Feulner, G., Bukenberger, M., & Petri, S. (2023). Tracing the snowball bifurcation of aquaplanets through time reveals a fundamental shift in critical-state dynamics. *Earth System Dynamics*, *14*(3), 533–547. https://doi.org/10.5194/esd-14-533-2023

Feulner, G., Hallmann, C., & Kienert, H. (2015). Snowball cooling after algal rise. *Nature Geoscience*, *8*(9), 659–662. https://doi.org/10.1038/ngeo2523

Feulner, G., & Kienert, H. (2014). Climate simulations of Neoproterozoic snowball Earth events: Similar critical carbon dioxide levels for the Sturtian and Marinoan glaciations. *Earth and Planetary Science Letters*, *404*, 200–205. https://doi.org/10.1016/j.epsl.2014.08.001

Fichefet, T., & Morales Maqueda, M. A. (1997). Sensitivity of a global sea ice model to the treatment of ice thermodynamics and dynamics. *Journal of Geophysical Research*, *102*(C6), 12609–12646. https://doi.org/10.1029/97JC00480

Green, J. A. M. (2010). Ocean tides and resonance. *Ocean Dynamics*, *60*(5), 1243–1253. https://doi.org/10.1007/s10236-010-0331-1

Green, J. A. M., Davies, H. S., Duarte, J. C., Creveling, J. R., & Scotese, C. (2020). Weak tides during Cryogenian glaciations. *Nature Communications*, *11*(1), 6227. https://doi.org/10.1038/s41467-020-20008-3

Green, J. A. M. & Duarte, J. C. (Eds.) (2022). *A journey through tides*. Elsevier.

Green, J. A. M., & Huber, M. (2013). Tidal dissipation in the early Eocene and implications for ocean mixing. *Geophysical Research Letters*, *40*(11), 2707–2713. https://doi.org/10.1002/grl.50510

Green, J. A. M., Huber, M., Waltham, D., Buzan, J., & Wells, M. (2017). Explicitly modelled deep-time tidal dissipation and its implication for Lunar history. *Earth and Planetary Science Letters*, *461*, 46–53. https://doi.org/10.1016/j.epsl.2016.12.038

Green, J. A. M., Molloy, J. L., Davies, H. S., & Duarte, J. C. (2018). Is there a tectonically driven supertidal cycle? *Geophysical Research Letters*, *45*(8), 3568–3576. https://doi.org/10.1002/2017GL076695

Green, J. A. M., & Nycander, J. (2013). A comparison of internal wave drag parameterizations for tidal models. *Journal of Physical Oceanography*, *43*(1), 104–119. https://doi.org/10.1175/jpo-d-12-023.1

Hawkesworth, C. J., Cawood, P. A., & Dhuime, B. (2020). The evolution of the continental crust and the onset of plate tectonics. *Frontiers in Earth Science*, *8*. https://doi.org/10.3389/feart.2020.00326

Heller, R., Duda, J.-P., Winkler, M., Reitner, J., & Gizon, L. (2021). Habitability of the early Earth: Liquid water under a faint young Sun facilitated by strong tidal heating due to a closer Moon. *PalZ*, *95*(4), 563–575. https://doi.org/10.1007/s12542-021-00582-7

Hofmann, M., & Morales Maqueda, M. A. (2006). Performance of a second-order moments advection scheme in an ocean general circulation model. *Journal of Geophysical Research*, *111*(C5), C05006. https://doi.org/10.1029/2005JC003279

Jermyn, A. S., Bauer, E. B., Schwab, J., Farmer, R., Ball, W. H., Bellinger, E. P., et al. (2023). Modules for experiments in stellar astrophysics (MESA): Time-dependent convection, energy conservation, automatic differentiation, and infrastructure. *The Astrophysical Journal*, *265*(1), 15. https://doi.org/10.3847/1538-4365/acae8d

Kienert, H., Feulner, G., & Petoukhov, V. (2012). Faint young Sun problem more severe due to ice-albedo feedback and higher rotation rate of the early Earth. *Geophysical Research Letters*, *39*(23), L23710. https://doi.org/10.1029/2012GL054381

Kienert, H., Feulner, G., & Petoukhov, V. (2013). Albedo and heat transport in 3-D model simulations of the early Archean climate. *Climate of the Past*, *9*(4), 1841–1862. https://doi.org/10.5194/cp-9-1841-2013

Klatt, J. M., Chennu, A., Arbic, B. K., Biddanda, B. A., & Dick, G. J. (2021). Possible link between Earth's rotation rate and oxygenation. *Nature Geoscience*, *14*(8), 564–570. https://doi.org/10.1038/s41561-021-00784-3

MacDonald, G. J. F. (1964). Tidal friction. *Reviews of Geophysics*, *2*(3), 467–541. https://doi.org/10.1029/RG002i003p00467

Montoya, M., Griesel, A., Levermann, A., Mignot, J., Hofmann, M., Ganopolski, A., & Rahmstorf, S. (2005). The earth system model of intermediate complexity CLIMBER-3α. Part I: Description and performance for present-day conditions. *Climate Dynamics*, *25*(2), 237–263. https://doi.org/10.1007/s00382-005-0044-1

Pacanowski, R. C., & Griffies, S. M. (1999). *The MOM-3 manual (Tech. Rep. No. 4)*. NOAA/Geophyical Fluid Dynamics Laboratory. Retrieved from https://mom-ocean.github.io/assets/pdfs/MOM3_manual.pdf

Petoukhov, V., Ganopolski, A., Brovkin, V., Claussen, M., Eliseev, A., Kubatzki, C., & Rahmstorf, S. (2000). CLIMBER-2: A climate system model of intermediate complexity. Part I: Model description and performance for present climate. *Climate Dynamics*, *16*(1), 1–17. https://doi.org/10.1007/pl00007919

Pollack, H. N., Hurter, S. J., & Johnson, J. R. (1993). Heat flow from the Earth's interior - Analysis of the global data set. *Reviews of Geophysics*, *31*(3), 267–280. https://doi.org/10.1029/93RG01249

Sawada, H. (2020). Estimation of secular change in the size of continents for understanding early crustal development. *Frontiers in Earth Science*, *8*. https://doi.org/10.3389/feart.2020.541094

Schmittner, A., Green, J. A. M., & Wilmes, S.-B. (2015). Glacial ocean overturning intensified by tidal mixing in a global circulation model. *Geophysical Research Letters*, *42*(10), 4014–4022. https://doi.org/10.1002/2015GL0635610

Sharples, J., Tweddle, J., Green, J., Palmer, M., Kim, Y.-N., Hickman, A., et al. (2007). Spring-neap modulation of internal tide mixing and vertical nitrate fluxes at a shelf edge in summer. *Limnology & Oceanography*, *52*(5), 1735–1747. https://doi.org/10.4319/lo.2007.52.5.1735

Tuerena, R., Williams, R., Mahaffey, C., Vic, C., Green, J., Naveira-Garabato, A., et al. (2019). Internal tides drive nutrient fluxes into the deep chlorophyll maximum over mid-ocean ridges. *Global Biogeochemical Cycles*, *33*(8), 995–1009. https://doi.org/10.1029/2019GB006214

Turcotte, D. L., & Schubert, G. (2002). *Geodynamics* (p. 456). Cambridge University Press.

Wilmes, S.-B., Green, J. A. M., & Schmittner, A. (2021). Enhanced vertical mixing in the glacial ocean inferred from sedimentary carbon isotopes. *Nature Communications Earth and Environment*, *2*(166), 166. https://doi.org/10.1038/s43247-021-00239-y

Wunsch, C., & Ferrari, R. (2004). Vertical mixing, energy, and the general circulation of the oceans. *Annual Review of Fluid Mechanics*, *36*(1), 281–314. https://doi.org/10.1146/annurev.fluid.36.050802.122121

Yang, J., Boué, G., Fabrycky, D. C., & Abbot, D. S. (2014). Strong dependence of the inner edge of the habitable zone on planetary rotation rate. *The Astrophysical Journal Letters*, *787*(1), L2. arXiv: 1404.4992. https://doi.org/10.1088/2041-8205/787/1/L2

Zahnle, K., Arndt, N., Cockell, C., Halliday, A., Nisbet, E., Selsis, F., & Sleep, N. H. (2007). Emergence of a habitable planet. *Space Science Reviews*, *129*(1), 35–78. https://doi.org/10.1007/s11214-007-9225-z

Zaron, E. D., & Egbert, G. D. (2006). Estimating open-ocean barotropic tidal dissipation: The Hawaiian Ridge. *Journal of Physical Oceanography*, *36*(6), 1019–1035. https://doi.org/10.1175/jpo2878.1